Near-Field Frequency-Domain Theory for Propeller Noise

Donald B. Hanson*
Hamilton Standard, Windsor Locks, Connecticut

Near-field noise equations are developed from the author's helicoidal surface theory for propeller aerodynamics and noise. Thickness, steady loading, and quadrupole sources are included. Apart from the thin-blade approximation and neglect of radial source terms, the equations are exact. In a comparison with the previously published far-field theory, it is shown that several valuable features of the far-field equations are retained. In particular, blade sweep still appears explicitly as a phase lag effect. A brief correlation with test data is shown.

Nomenclature

b = airfoil chord
B = number of blades
B_D = chord-to-diameter ratio, $= b/D$.
c_0 = ambient speed of sound
C_L = lift coefficient
C_D = drag coefficient
D = propeller diameter
FA = face alignment or offset, see Fig. 2
g = generalized source function, Eq. (4)
h = thickness distribution; also, phase factor in Appendix
H = normalized thickness distribution (Fig. 3), $= h/b$
J_n = Bessel function
k = $\bar{\omega}/mB\Omega$
k_x, k_y = wave numbers given by Eqs. (7) and (8)
m = harmonic of blade passing frequency
MCA = midchord alignment or sweep, see Fig. 2
M_r = section relative Mach number, $= \sqrt{M_x^2 + z^2 M_T^2}$
M_T = tip rotational Mach number, $= \Omega r_T / c_0$
M_x = flight Mach number, $= V/c_0$
n = harmonic of shaft frequency, $= mB$
p = acoustic pressure
P_{mB} = complex Fourier coefficient of p
r, r_0 = distance from axis to observer point, source point
r = distance from origin to observer (in Appendix only)
r_T = propeller tip radius, $= D/2$
t = time
t_b = ratio of maximum thickness to chord
T_{ij} = quadrupole source
U_0 = local blade section speed, $= \sqrt{V^2 + \Omega^2 r_0^2}$
V = flight speed
x = distance ahead of propeller radiation position
x_1 = distance ahead of propeller visual position
X = normalized chordwise coordinate, $= \gamma_0 / b$
y = observer distance from propeller axis
Y = normalized coordinate perpendicular to chord and radius, $= \xi_0 / b$
z = normalized radial coordinate, $= r_0 / r_T$
γ_0 = source coordinate in chordwise direction (Fig. 2)
δ = Dirac delta (impulse) function
θ = radiation angle from propeller axis to observer point
ξ_0 = source coordinate normal to chord (Fig. 2)
ρ_0 = ambient density
Σ' = zeroth term omitted
ϕ_o, ϕ_s = phase lag due to offset and sweep, Eqs. (25) and (26)
ϕ_x = phase lag associated with observer
$\bar{\omega}$ = integration variable
Ω = 2π times shaft rotation frequency
$( )'$ = differentiation with respect to argument, as in h'

Presented as Paper 83-0688 at the AIAA Eighth Aeroacoustics Conference, Atlanta, Ga., April 11-13, 1983; received May 8, 1983; revision received June 11, 1984. Copyright © American Institute of Aeronautics and Astronautics, Inc., 1983. All rights reserved.

*Principal Research Engineer, Design Department, Aircraft Systems Division. Member AIAA.

Introduction

THE prop fan shown in Fig. 1 is under development for fuel-conservative aircraft of the 1990s. Because it operates at subsonic tip speeds on takeoff and landing, the community noise from this type of propeller is expected to be acceptable. However, in cruise the tip helical speed may be as high as Mach 1.15. Since this may cause a cabin noise problem, accurate near-field prediction methods are needed for analysis and design.

The noise radiation formulas presented herein are cast directly in the frequency domain so that harmonics are computed one at a time. This is particularly advantageous for prop fans where often only the fundamental harmonic is of interest. Waveforms, if needed, can be computed by constructing the Fourier series from several harmonics. The time-domain methods developed for this application also have merit. Since they have been surveyed recently by Farassat,[1] they will not be discussed further here.

The noise theory given below is a branch of a more general helicoidal surface theory derived by the author[2] that includes steady and unsteady aerodynamics as well. It is based on the acoustic analogy and is made particularly tractable by recognizing that each source element travels in a helical path.

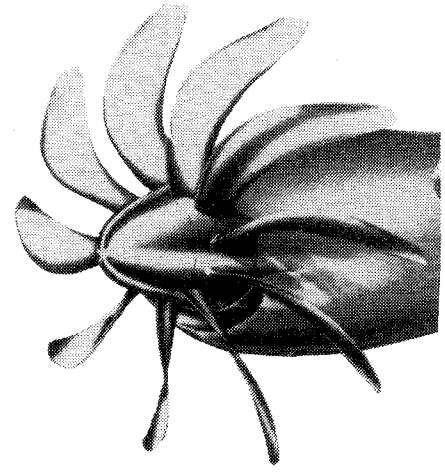

Fig. 1 Propfan propulsor.

The only approximation made is that the blades are thin; i.e., all portions of the airfoil section at a given radius lie much closer than a wavelength to the helix corresponding to that radius. Since this applies for 50 or more harmonics, it is quite satisfactory for prop fans. Noise sources (thickness and loading) are represented by their spatial Fourier transforms in the chordwise direction as in the author's far-field propeller noise theory.[3] Transformation to the frequency domain eliminates any need to calculate retarded source positions.

Background

In Ref. 2 the density disturbance ρ' caused by any helically convected steady source distribution was shown to be given by

$$c_0^2\rho'(x_1,r,\phi,t)=\frac{i}{8\pi V}\sum_{n=-\infty}^{\infty}\exp[in(\phi-\Omega t]$$
$$\times\int_0^{\infty}\int_{-\infty}^{\infty}\exp[i(\tilde{\omega}-n\Omega)x_1/V]J_n(\mu r_0)H_n^{(1)}(\mu r)$$
$$\times\int_{-\infty}^{\infty}\psi\left(\frac{\tilde{\omega}}{U_0},\xi_0,r_0\right)\exp\left[-i(\tilde{\omega}-n\Omega)\frac{\Omega r_0\xi_0}{VU_0}\right]$$
$$\times\exp[in(V\xi_0/r_0U_0)]\,d\xi_0\,d\tilde{\omega}\,dr_0 \qquad (1)$$

where

$$\mu=\sqrt{\left(\frac{\tilde{\omega}}{c_0}\right)^2-\left(\frac{\tilde{\omega}-n\Omega}{V}\right)^2} \qquad (2)$$

The source coordinates r_0, ζ_0, and γ_0 are shown in Fig. 2. ζ_0 and γ_0 are measured in the cylindrical surface $r_0=$ const and cross each other at right angles. The flight speed is V and the local section helical speed is $U_0=\sqrt{V^2+\Omega^2r_0^2}$. ψ is the transform of the source distribution defined by

$$\psi(\tilde{\omega}/U_0,\xi_0,r_0)=\int_{-\infty}^{\infty}g(\gamma_0,\xi_0,r_0)\exp(i\tilde{\omega}\gamma_0/U_0)\,d\gamma_0 \qquad (3)$$

and g is the generalized source function

$$g(\gamma_0,\xi_0,r_0)=\left[\rho_0U_0^2\frac{\partial^2}{\partial\gamma_0^2}h(\gamma_0,r_0)+\frac{\partial}{\partial\gamma_0}D(\gamma_0,r_0)\right.$$
$$\left.+\frac{\partial}{\partial r_0}F_r(\gamma_0,r_0)\right]\delta(\xi_0+\mathrm{FA})+\Delta P(\gamma_0,r_0)\delta'(\xi_0+\mathrm{FA})$$
$$+\frac{\partial^2}{\partial y_i\partial y_j}T_{ij}(\gamma_0,\xi_0,r_0) \qquad (4)$$

The individual sources are h, the thickness distribution; D, F_r, and ΔP, the drag, radial force, and lift force per unit blade area, respectively and T_{ij}, the acoustic stress tensor. The delta function, $\delta(\xi_0,+\mathrm{FA})$ places the surface sources on the advance helix given by $\xi_0=-\mathrm{FA}$ as shown in Fig. 2.

In Ref. 2, Eq. (1) was linearized and developed into a velocity potential for aerodynamic applications. In the following section, however, it is adapted directly to acoustics and the nonlinear source term T_{ij} is retained.

Normalized Equations

In this section, Eq. (1) is rewritten in terms of Mach numbers and normalized coordinates. Also, the generalized frequency-domain source function ψ is expressed in explicit form for convenient computation.

Outside the transonic flowfield of the rotor, if any, the acoustic pressure disturbance is given by

$$p=c_0^2\rho' \qquad (5)$$

Therefore, Eq. (1) gives the pressure field of a one-bladed rotor in terms of a harmonic series in n. For a rotor with B blades the harmonics of order mB reinforce in phase and the harmonics corresponding to other values of n cancel with the result

$$p=\sum_{m=-\infty}^{\infty}{}'P_{mB}\exp[imB(\phi-\Omega t)] \qquad (6)$$

To find the harmonics P_{mB}, a normalized frequency integration variable k is defined according to $\tilde{\omega}=mB\Omega k$ and two wave numbers are defined for convenience:

$$k_x=\frac{2mBB_DM_Tk}{M_r} \qquad (7)$$

$$k_y=\frac{2mBB_D}{zM_xM_r}(M_r^2-kz^2M_T^2) \qquad (8)$$

so that $\tilde{\omega}\gamma_0/U_0$ in Eq. (3) can be written k_xX, where $X=\gamma_0/b$. Similarly, the exponents containing ξ_0 in Eq. (1) can be written $\exp(ik_yY)$ where $Y=\xi_0/b$. $B_D=b/2r_T$ is the local chord-to-diameter ratio. Also, the phase angle associated with x_1 is written

$$\phi_x=\frac{2mBM_T(k-1)}{M_x}\frac{x_1}{D} \qquad (9)$$

With this new notation the sound harmonic becomes

$$P_{mB}=\frac{imB^2M_T}{8\pi M_x}\int_0^{\infty}\int_{-\infty}^{\infty}e^{i\phi_x}J_nH_n^{(1)}\int_{\infty}^{\infty}\psi\exp(ik_y\xi_0/b)\,d\xi_0\,dk\,dz \qquad (10)$$

where the radius ratio $z=r_0/r_T$ extends, in principle, to infinity for the volume sources but ends at unity for the surface sources.

We now concentrate on the inner integral from Eq. (10)

$$I_s=\int_{-\infty}^{\infty}\psi\exp(ik_y\xi_0/b)\,d\xi_0 \qquad (11)$$

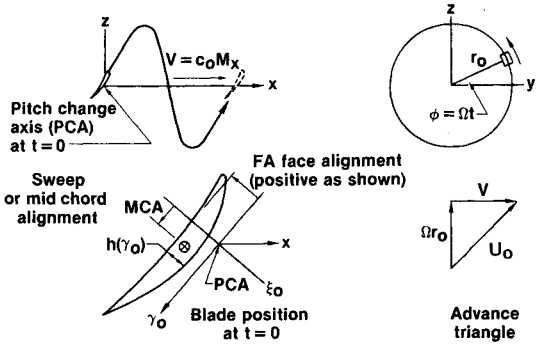

Fig. 2 Blade element shown in helical coordinates.

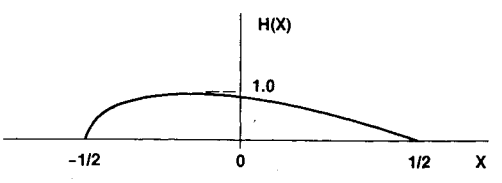

Fig. 3 Normalized thickness distributions.

which, with Eq. (3), becomes

$$I_s = \int\int g(\gamma_0,\xi_0,r_0)\exp(ik_x\gamma_0/b)\exp(ik_y\xi_0/b)\,d\gamma_0 d\xi_0 \qquad (12)$$

The source term g is substituted from Eq. (4) with the radial force term F_r and radial derivatives of T_{ij} neglected.

$$\begin{aligned} I_s = {} & \rho_0 U_0^2 \int \frac{\partial^2}{\partial\gamma_0^2} h(\gamma_0,r_0)\exp(ik_x\gamma_0/b)\,d\gamma_0 \\ & \times \int \delta(\xi_0+\mathrm{FA})\exp(ik_y\xi_0/b)\,d\xi_0 \\ & + \int \frac{\partial}{\partial\gamma_0} D(\gamma_0,r_0)\exp(ik_x\gamma_0/b)\,d\gamma_0 \\ & \times \int \delta(\xi_0+\mathrm{FA})\exp(ik_y\xi_0/b)\,d\xi_0 \\ & + \int \Delta P(\gamma_0,r_0)\exp(ik_x\gamma_0/b)\,d\gamma_0 \\ & \times \int \delta'(\xi_0+\mathrm{FA})\exp(ik_y\xi_0/b)\,d\xi_0 + \int\int \frac{\partial^2}{\partial y_i y_j} T_{ij}(\gamma_0,\xi_0,r_0) \\ & \times \exp(ik_x\gamma_0/b)\exp(ik_y\xi_0/b)\,d\gamma_0 d\xi_0 \end{aligned} \qquad (13)$$

The integrals of the first two delta functions yield $\exp(i\phi_o)$ where $\phi_o = -k_y\mathrm{FA}/b$ is the phase angle associated with blade face alignment, FA. The integral of δ' is performed by parts, yielding $(-ik_y/b)\exp(i\phi_o)$. Similar integrations by parts are used for the γ_0 integrals and the implied summations an i and j are carried out with the result

$$\begin{aligned} I_s = {} & \rho_0 U_0^2 \exp[i\phi_o]\left(\frac{-k_x^2}{b^2}\right)\int h(\gamma_0,r_0)\exp(ik_x\gamma_0/b)\,d\gamma_0 \\ & - \exp[i\phi_o]\left(\frac{ik_x}{b}\right)\int D(\gamma_0,r_0)\exp(ik_x\gamma_0/b)\,d\gamma_0 \\ & - \exp[i\phi_o]\left(\frac{ik_y}{b}\right)\int \Delta P(\gamma_0,r_0)\exp(ik_x\gamma_0/b)\,d\gamma_0 \\ & - \frac{k_x^2}{b^2}\int\int T_{11}(\gamma_0,\xi_0,r_0)\exp(ik_x\gamma_0/b)\exp(ik_y\xi_0/b)\,d\gamma_0 d\xi_0 \\ & - 2\frac{k_x k_y}{b^2}\int\int T_{12}(\gamma_0,\xi_0,r_0)\exp(ik_x\gamma_0/b) \\ & \times \exp(ik_y\xi_0/b)\,d\gamma_0 d\xi_0 \\ & - \frac{k_y^2}{b^2}\int\int T_{22}(\gamma_0,\xi_0,r_0)\exp(ik_x\gamma_0/b)\exp(ik_y\xi_0/b)\,d\gamma_0 d\xi_0 \end{aligned} \qquad (14)$$

Now, as in Ref. 3, the airfoil section thickness distribution h is expressed in terms of the normalized shape function H shown in Fig. 3 as

$$h(\gamma_0,r_0) = bt_b H\left(X - \frac{\mathrm{MCA}}{b}\right) \qquad (15)$$

The appearance of MCA in the argument of H accounts for the section sweep as in Fig. 2. Similarly, the drag and lift force distributions are expressed in terms of their coefficients C_D and C_L and functions f_D and F_L whose areas are unity and whose shapes give the chordwise distributions. Thus,

$$D(\gamma_0,r_0) = \frac{\rho_0 U^2}{2} C_D f_D\left(X - \frac{\mathrm{MCA}}{b}\right) \qquad (16)$$

$$\Delta P(\gamma_0,r_0) = \frac{\rho_0 U^2}{2} C_L f_L\left(X - \frac{\mathrm{MCA}}{b}\right) \qquad (17)$$

Finally, the T_{ij} components are shifted to airfoil coordinates according to

$$T_{ij}(\gamma_0,\xi_0,r_0) \rightarrow T_{ij}\left(X - \frac{\mathrm{MCA}}{b}, Y + \frac{\mathrm{FA}}{b}, z\right) \qquad (18)$$

Substitution of these equations into Eq. (14) and shifting the X variable by MCA/b gives

$$\begin{aligned} I_s = {} & -\rho_0 U_0^2 \exp[i(\phi_o+\phi_s)]\left[k_x^2 t_b \Psi_v(k_x) + ik_x\frac{C_D}{2}\Psi_D(k_x)\right. \\ & \left. + ik_y\frac{C_L}{2}\Psi_L(k_x) + \Psi_Q(k_x,k_y)\right] \end{aligned} \qquad (19)$$

where the frquency-domain surface sources are

$$\begin{Bmatrix} \Psi_V(k_x) \\ \Psi_D(k_x) \\ \Psi_L(k_x) \end{Bmatrix} = \int_{-1/2}^{1/2} \begin{Bmatrix} H(x) \\ f_D(x) \\ f_L(x) \end{Bmatrix} \exp[ik_x X]\,dX \qquad (20)$$

and the quadrupole source is

$$\Psi_Q = k_x^2\Psi_{11} + 2k_x k_y \Psi_{12} + k_y^2 \Psi_{22} \qquad (21)$$

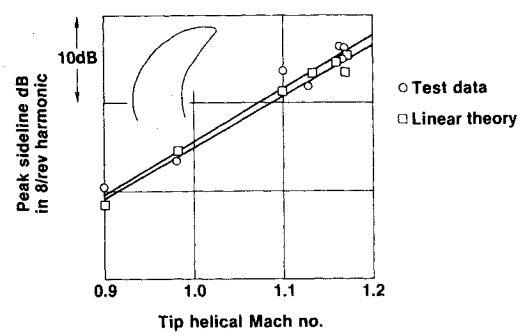

Fig. 4 Comparison of test data with prediction of near-field theory.

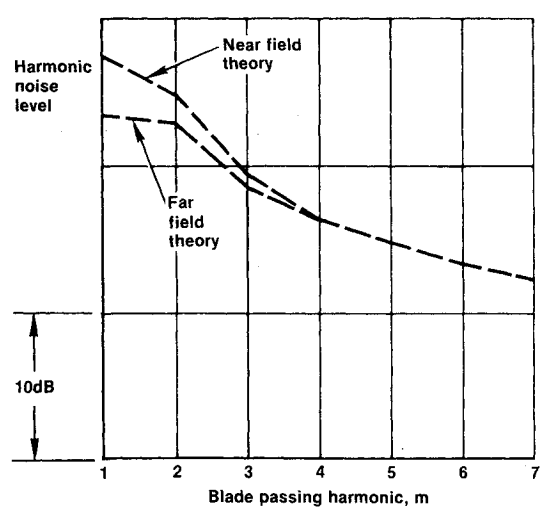

Fig. 5 Comparison of prediction from near- and far-field theories for an observer at 0.8D tip clearance. Tip helical Mach number = 1.15.

with

$$\Psi_{ij}(k_x,k_y)=\int\int\frac{T_{ij}}{\rho_0 U_0^2}\exp[ik_xX]\exp[ik_yY]\,dX\,dY \quad (22)$$

The phase lag due to sweep $\phi_s=k_x\mathrm{MCA}/b$ was discussed in some detail in Ref. 4 in conjunction with the far-field theory.

The inner integral I_s from Eq. (19) now can be replaced in Eq. (10) for the final radiation formulas.

$$\left\{\begin{matrix}P_{Vm}\\P_{Dm}\\P_{Lm}\\P_{Qm}\end{matrix}\right\}=\frac{-i\rho_0c_0^2mB^2M_T}{8\pi M_x}$$

$$\times\int_{z_{\mathrm{root}}}^{z_{\mathrm{tip}}}M_r^2\int_{-\infty}^{\infty}\exp[i(\phi_o+\phi_s+\phi_x)]$$

$$\times J_{mB}\left[\frac{mBzM_T}{M_x}\sqrt{M_x^2k^2-(k-l)^2}\right]$$

$$\times H_{mB}^{(l)}\left[\frac{2mBM_T}{M_x}\frac{y}{D}\sqrt{M_x^2k^2-(k-l)^2}\right]$$

$$\times\left\{\begin{matrix}k_x^2t_b\Psi_V(k_x)\\ik_x(C_D/2)\Psi_D(k_x)\\ik_y(C_L/2)\Psi_L(k_x)\\\Psi_Q(k_x,k_y)\end{matrix}\right\}dk\,dz \quad (23)$$

where

$$P_{mB}=P_{Vm}+P_{Dm}+P_{Lm}+P_{Qm} \quad (24)$$

and the face alignment and sweep phase angles can be written as

$$\phi_o=\frac{2mB}{z}\frac{kz^2M_T^2-M_r^2}{M_xM_r}\frac{\mathrm{FA}}{D} \quad (25)$$

$$\phi_s=\frac{2mBM_Tk}{M_r}\frac{\mathrm{MCA}}{D} \quad (26)$$

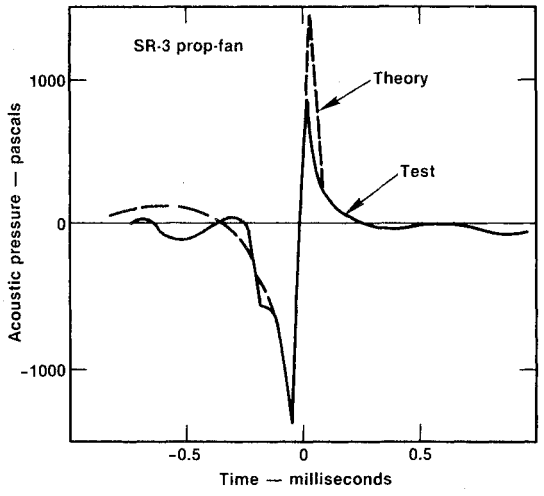

Fig. 6 Waveform calculated with frequency domain theory compared with data. Tip relative Mach number = 1.211; tip clearance, 0.8 diameter.[6]

A partial verification of Eq. (23) can be obtained by passing to the far field and comparing with previous results. For large enough y, the large-argument asymptotic form for $H_{mB}^{(l)}$ can be used and the integral k can be evaluated by the stationary phase method. As shown in Appendix A for the P_{Vm} component, for example, the far-field limit of Eq. (23) is

$$P_{Vm}\xrightarrow[\text{field}]{\text{Far-}}\frac{-\rho_0c_0^2B\sin\theta}{8\pi(y/D)(1-M_x\cos\theta)}\exp\left[imB\left(\frac{\Omega r}{c_0}-\frac{\pi}{2}\right)\right]$$

$$\times\int_0^l M_r^2\exp[i(\phi_o+\phi_s)]J_{mB}\left(\frac{mBzM_T\sin\theta}{1-M_x\cos\theta}\right)k_x^2t_b\Psi_V(k_x)\,dz \quad (27)$$

This is exactly the same form as was found in Ref. 3 via a direct far-field derivation with the exception that the term $\Omega r/c_0$ in the phase factor outside the integral was $\Omega_D r/c_0$, where $\Omega_D=\Omega/(1-M_x\cos\theta)$. The difference of a Doppler factor is as it should be because the original far-field formulas were derived for a stationary observer, whereas the present equations apply to an observer translating with the propeller.

Properties of Near-Field Equation

The near-field noise formulas of Eq. (23) bear a strong resemblance to the far-field equations presented in Ref. 3.† The major difference is an extra integration that can be interpreted as a Fourier transform in the wave number variable k. Thus, the integrand represents the field of infinitely long wavy sources arrayed along the helical advance path of the airfoil section. These are reminiscent of the familiar wavy-wall problem in elementary aerodynamic texts. Integration over k synthesizes the field of the actual source distribution from its Fourier components.

A significant feature of Eq. (23) is the way in which the axial observer position variable x_l appears. Usually, in near-field calculations, it is desired to compute a directivity pattern at constant distance y from the propeller axis. To accomplish this using Eq. (23), the k integration is done via a fast Fourier Transform so that the directivity pattern is returned as the transformed array in the variable x_l.

The Ψ functions can be generated in various ways. For approximate work, idealized source functions can be used such as a biconvex thickness shape for $H(x)$ and a constant for the loading function f_L. These can be transformed analytically and give useful results for lower harmonics of conventional propellers. Another approach is simply to perform the Ψ transforms during the noise calculations; however, this is cumbersome for a production computer program. A more practical system and the one in use at Hamilton Standard is to precompute a large family of the Ψ's, typically with a two-dimensional transonic airfoil code, and store them on a disk. This results in a system that can compute an entire directivity pattern for the blade passing fundamental of a propfan quickly enough for production running of the program.

Harmonic Predictions

The system described previously has been used at Hamilton Standard for propfan prediction since 1977 with the linear source terms. Quadrupole sources[5] were added in 1979. Agreement with test data is generally good and has been documented in Ref. 6. A summary curve comparing near-field test and theory for the SR-3 propfan in the United Technologies Acoustic Research Tunnel is given in Fig. 4. The curve represents the maximum sideline level at 0.8 diam tip

†In comparing the above near-field formulas with the far-field theory of Refs. 3 and 4, the reader should note a change in the sign convention for k_y as described in Appendix B.

clearance for the blade passing frequency of an eight-bladed propeller. Calculations were performed without quadrupole sources, which are weak for highly swept blades. (A discussion of the influence of sweep on shock formation and other nonlinear effects is given in Ref. 7.) Further comparisons with data are given by Metzger[8] for flight tests of a model propfan.

Waveform Predictions

In principle, near-field waveforms can be predicted using the Fourier series of Eq. (6) with coefficients given by Eq. (23). However, for high-speed propellers with many contributing harmonics, this would be prohibitive because the integrals require finer meshes as harmonic order increases. Fortunately, Eq. (23) can be simplified by the method of stationary phase for the higher harmonics so that waveform calculations become practical.

In Appendix A, it is shown that, for large values of the parameter mBr/D, the wave number integration can be performed analytically and the equation simplifies essentially to the far-field noise theory, where only a radial integration is required. Fig. 5 gives a comparison of near-field harmonic levels as predicted for a prop fan by both the near- and far-field theories. Typically, the results are the same after the third harmonic.

A waveform computed from the frequency-domain theory is shown in Fig. 6. Comparison with a microphone signal is generally very good. The positive pressure spike, which is caused by recompression of flow at the blade trailing edge, appears to be smeared by the airfoil boundary layer or nonlinear propagation. These effects have not been included in the calculation because the details of the pressure spike do not greatly influence the fundamental harmonic.

Conclusions

Equations have been presented for the near-field noise of propellers with steady loading in forward flight. Many features of the author's far-field theory are retained. In particular, the phase lags ϕ_s and ϕ_o due to sweep and offset appear explicitly and the sources are represented by their spatial Fourier transforms.

In the near-field, an additional wave number integral appears in such a way that entire directivity patterns can be computed at once. For harmonic order above about 3 for propfans, the integral can be evaluated with good accuracy with the method of stationary phase. This permits calculation of waveforms by harmonic synthesis.

The theory has proved to be efficient in use of computer time and accurate for both design and analysis applications. Trends of harmonic level with tip Mach number measured in the United Technologies Research Center Acoustic Research Tunnel are predicted well and major waveform features are explained.

Appendix A: Derivation of Far-Field Equation

Equation (23) contains a Hankel function that may be replaced by an asymptotic form when its argument becomes large, thereby permitting the k integral to be evaluated by the method of stationary phase.[9] The result recovers the far-field formulas as shown below by example for P_{Vm}.

By the stationary phase method, integrals of the form

$$I=\int_{-\infty}^{\infty} g(t)\exp[i\alpha h(k)]\,dk \tag{A1}$$

can be evaluated for $\alpha\to\infty$ according to

$$I\to\left|\frac{2\pi}{\alpha h''(k_0)}\right|^{1/2} g(k_0)\exp\left\{i\left[\alpha h(k_0)\pm\frac{\pi}{4}\right]\right\} \tag{A2}$$

where k_0 is the stationary phase point given by $h'(k_0)=0$ and the $\pm$ sign goes as the sign of $h''(k_0)$.

Upon substituting the asymptotic form

$$H_{mB}^{(1)}(z)\to\sqrt{\frac{2}{\pi z}}\exp\left\{i\left[z-\frac{mB\pi}{2}-\frac{\pi}{4}\right]\right\} \tag{A3}$$

and the definitions for ϕ_o, ϕ_s, ϕ_x, and k_x into Eq. (23), the k integral becomes

$$I_V=\int\exp[i(\phi_o+\phi_s)]J_{mB}k_x^2t_b\Psi_V(k_x)\sqrt{\frac{M_x}{\pi mBM_T(y/D)E}}$$
$$\times\exp[-i(mB\pi/2+\pi/4)]\exp[i\alpha h(k)]\,dk \tag{A4}$$

where

$$\alpha=\frac{2mBM_T}{M_x}\frac{r}{D} \tag{A5}$$

and

$$h=\frac{y}{r}E+(k-1)\frac{x_1}{r} \tag{A6}$$

with

$$E=\sqrt{M_x^2k^2-(k-1)^2} \tag{A7}$$

The derivation proceeds more conventiently in terms of the radiation angle θ than the coordinate x_1. It was shown in Ref. 4 for a retarded axial distance x and radiation distance r that

$$x_1/r=\cos\theta-M_x \tag{A8}$$

where

$$\cos\theta=x/r,\quad \sin\theta=y/r \tag{A9}$$

Then with the necessary derivatives and algebra, it is found that the stationary phase point is

$$k_0=1/(1-M_x\cos\theta) \tag{A10}$$

and

$$E(k_0)=(M_x\sin\theta)/(1-M_x\cos\theta) \tag{A11}$$

With these expressions the phase angle becomes

$$\alpha h(k_0)=mB\Omega r/c_0 \tag{A12}$$

The amplitude factor in the far field is

$$h''(k_0)=-[(1-M_x\cos\theta)^3]/(M_x\sin^2\theta) \tag{A13}$$

Using these values to evaluate Eq. (A4) and substituting for the k integral in Eq. (23) gives

$$P_{Vm}\to\frac{-\rho_0c_0^2B\sin\theta}{8\pi(y/D)(1-M_x\cos\theta)}\exp\left[imB\left(\frac{\Omega r}{c}-\frac{\pi}{2}\right)\right]$$
$$\times\int_0^1 M_r^2\exp[i(\phi_o+\phi_s)]J_{mB}\left(\frac{mBzM_T\sin\theta}{1-M_x\cos\theta}\right)k_x^2t_b\Psi_v(k_x)\,dz \tag{A14}$$

for the exact far-field result.

Appendix B: Comparison with Far-Field Theory

In Refs. 3 and 4 the sign convention for the k_y wave number is different from the lift and the quadrupole noise sources. For consistency with the present paper, these references should be corrected as follows.

In Ref. 3, Eq. (42), change the sign in the definition of k_y. In Eq. (36) the minus sign in $-ik_y$ should be deleted. These

two changes affecting loading noise represent a change in sign convention only. The sign on k_y in the definition of the quadrupole transform in Eq. (41) should not be changed and, therefore, was in error before the change in convention.

In Ref. 4 the sign of k_y in Eqs. (1) and (6) should be changed—a difference in sign convention only.

References

[1]Farassat, F., "Linear Acoustic Formulas for Calculation of Rotating Blade Noise," *AIAA Journal*, Vol. 19, Sept. 1981, p. 1122.

[2]Hanson, D. B., "Compressible Helicoidal Surface Theory for Propeller Aerodynamics and Noise," *AIAA Journal*, Vol. 21, June 1983, p. 881.

[3]Hanson, D. B., "Helicoidal Surface Theory for Harmonic Noise of Propellers in the Far-Field," *AIAA Journal*, Vol. 18, Oct. 1980, p. 1213.

[4]Hanson, D. B., "Influence of Propeller Design Parameters on Far-Field Harmonic Noise in Forward Flight," *AIAA Journal*, Vol. 18, Nov. 1980, p. 1313.

[5]Hanson, D. B. and Fink, M. R., "The Importance of Quadrupole Sources in Prediction of High Speed Propeller Noise," *Journal of Sound and Vibration*, Vol. 62, No. 1, 1979, pp. 19-38.

[6]Brooks, B. M. and Metzger, F. B., "Acoustic Test and Analysis of Three Advanced Turboprop Models," NASA CR-159667, Jan. 1980.

[7]Hanson, D. B., "The Aeroacoustics of Advanced Turbopropellers," *Mechanics of Sound Generation in Flows*, Spring-Verlag, New York, 1979, pp. 282-293.

[8]Metzger, F. B., "Measurements and Predictions of Turboprop Noise in High Cruise Speed, AIAA Paper 83-0689, April 1983.

[9]Jeffreys, H. and Jeffreys, B. S., *Methods of Mathematical Physics*, Cambridge University Press, Cambridge, England, 1956.

From the AIAA Progress in Astronautics and Aeronautics Series...

ORBIT-RAISING AND MANEUVERING PROPULSION: RESEARCH STATUS AND NEEDS—v. 89

Edited by Leonard H. Caveny, Air Force Office of Scientific Research

Advanced primary propulsion for orbit transfer periodically receives attention, but invariably the propulsion systems chosen have been adaptations or extensions of conventional liquid- and solid-rocket technology. The dominant consideration in previous years was that the missions could be performed using conventional chemical propulsion. Consequently, major initiatives to provide technology and to overcome specific barriers were not pursued. The advent of reusable launch vehicle capability for low Earth orbit now creates new opportunities for advanced propulsion for interorbit transfer. For example, 75% of the mass delivered to low Earth orbit may be the chemical propulsion system required to raise the other 25% (i.e., the active payload) to geosynchronous Earth orbit; nonconventional propulsion offers the promise of reversing this ratio of propulsion to payload masses.

The scope of the chapters and the focus of the papers presented in this volume were developed in two workshops held in Orlando, Fla., during January 1982. In putting together the individual papers and chapters, one of the first obligations was to establish which concepts are of interest for the 1995-2000 time frame. This naturally leads to analyses of systems and devices. This open and effective advocacy is part of the recently revitalized national forum to clarify the issues and approaches which relate to major advances in space propulsion.

Published in 1984, 569 pp., 6×9, illus., $45.00 Mem., $72.00 List

TO ORDER WRITE: Publications Order Dept., AIAA, 1633 Broadway, New York, N.Y. 10019